2017 Joint International Conference on Materials Science and Engineering Application (ICMSEA 2017) and
International Conference on Mechanics, Civil Engineering and Building Materials (MCEBM 2017)
ISBN: 978-1-60595-448-6

Effect of Dislocation Density Gradient on Deformation Behavior of Pure Nickel Subjected to Torsion

Dong HE[1,a,*], Yong HUAN[2,b], and Qiang LI[1,c]

[1]North China University of Technology, No. 5 Jinyuanzhuang Road, Shijingshan Dist., Beijing, China

[2]Institute of Mechanics, Chinese Academy of Sciences, 15 BeiSiHuan West Road, Beijing, China

[a]hedong@ncut.edu.cn, [b]huany@lnm.imech.ac.cn, [c]liqiang@ncut.edu.cn

*Corresponding author

Keywords: Dislocation, Gradient, Deformation behavior, Work-hardening rate, Pure nickel.

Abstract. Gradient hierarchical structures, including grain size gradient, twin density gradient, and texture gradient, are believed to broke up the long-standing dilemma-"strength-ductility trade-off" in materials science. Here we study the effect of dislocation density gradient on deformation behavior of pure nickel subjected to torsion. After applying torsion to cylindrical pure nickel samples, we find that Vickers hardness gradually decreased from surface to centre and the there is no obvious grain size gradient along the radial direction. The compression tests have been conducted on samples with different thickness of gradient layers. The results indicate that the yielding strength of the material can be three-times improved. Especially, the work-hardening rate "up-turn" phenomenon which was usually found in gradient nano-structures is presented in the torsion deformed pure nickel. Finally, the possible reasons and the effect of thickness of gradient structure are carefully discussed.

Introduction

In comparison with conventional coarse-grained polycrystalline materials, nanocrystalline materials, composed by single or multi-phase polycrystals with nanoscale grain size, usually exhibit significantly increased (2~10 times) strength/hardness [1]. However, the nanomaterials also suffer from low ductility [2]. Further studies indicate that, the gradually weakened work-hardening ability is one possible reason account for the premature plastic instability of nano metal materials [3-6].

Recently, many research results indicate that the gradient microstructure, in which the grain size[7]/gradient hierarchical nanotwins[8] increases from nanoscale at the surface to coarse-grained in the core, can evade the strength-ductility trade-off dilemma through work-hardening ability re-obtaining. This special effect is also referred to as "gradient effect".

It is worth to note that many meaningful works have been conducted in recent years in gradient microstructure. Examples include grain size gradient [7, 9], layer thickness gradient[10], hierarchical nanotwins gradient[8, 11] or their mixed gradient structure[12]. The results indicate that gradient nanograined, gradient nanotwinned structure can result an extra strain hardening and obtain an exceptionally superior strength ductility combinations. However, few works have been carried out to investigate the only dislocation density gradient effect on deformation behavior.

In the current paper, we focus on the dislocation density gradient introduced by torsion deformation effects on deformation behavior of pure nickel. The rest of the paper is arranged as follows. Firstly, torsion deformations with different torsion angle to cylindrical pure nickel samples have been performed. Then, the microstructures have been characterized by combination of metallographic and EBSD observation. Finally, compression deformations have and been conducted and deformation behaviors have been summarized.

Experimental Procedure

Materials and Sample Preparation

The pure nickel (Ni>99.5%) is used in the current study. The used materials are completely annealed at 600℃ for 2 hours. The microstructure of annealed nickel consisted of equiaxed coarse grains with 70-95 μm diameters (See Fig.1 a).

Dog-bone–shaped torsional bar specimens with a gauge diameter of 12.5mm and gauge length of 20mm were machined along the elongated direction from the annealed nickel, as shown in Fig. 1 b.

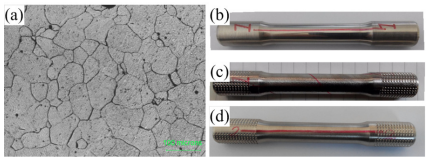

Figure 1. (a) Metallographic microstructure of pure nickel annealed at 600℃. (b) Photos of dog-bone-shaped torsional bar before torsional deformation. (c) With 360° torsion. (d) With 720° torsion (twisted 360° and untwisted 360°).

Torsional Deformation

Annealed nickel specimens are twisted in a lathe. The surface shear strain γ is given by

$$\gamma = R\theta / l \quad (1)$$

Where R is the specimen radius, θ is the rotation in radians and l is the length of the twisted region.

In order to take the influence of shear strain into consideration, the sample with different torsion angles are prepared. Sample A and B are twisted through 360° and 720°(twisted 360° and untwisted 360°), respectively. The resultant strain is equivalent to that produced in a unidirectional twist [13]. The detailed parameters are listed in Table1. The torque versus twist curve is given in Fig. 2.

Table 1. Detailed parameters for torsional deformation.

Sample No.	*R*, mm	*l*, mm	Torsion angle	Surface shear strain
A	6.25	50	360°	1.57
B	6.25	40	720°(360°/-360°)	3.14

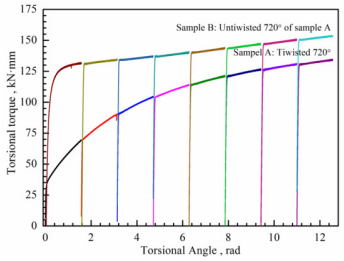

Figure 2. Torque versus twist curves of sample A and sample B.

Microstructure and Micro-hardness Measurements

Microstructures of torsioned samples are examined by metallographic and EBSD techniques. For this purpose, the cross sections of torsioned samples are prepared through standard grinding and polishing routines (ASTM: ASTM E3-11). The final polishing with a polishing solution consisting of colloidal silica (OP-S, 90 vol.%) and H2O2 (10 vol.%) was performed.

EBSD measurements were carried out on a JEOL 6500F scanning electron microscope equipped with an EBSD system developed by EDAX/TSL. To facilitate comparison, the top surface region,

subsurface region and centre region of each torsioned specimen are selected for microstructure observation.

Micro-hardness measurements along the radial direction are conducted on FV-800Vickers. 25gf force with 10 seconds holding time is applied for per indention test.

Uniaxial Compression Test

To investigate the different gradient compositions effect on deformation behavior, compression specimens with different diameters are machined along the axial direction from the torsioned nickel samples, as shown in Fig. 3. It is worth noting that the same aspect ratios (l/d=2) are adopted for all compression specimens to facilitate comparison. The detailed parameters of compression specimens are listed in Table2.

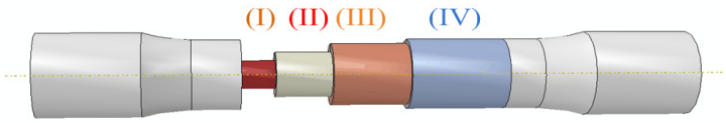

Figure 3. The sketch map of compression sample machined from the dog-bone-shaped bar after torsion deformation, the aspect ratios are same(l/d=2) and the diameters (d) are 5, 8, 11 and 12.5mm for sample I, II, III, IV, respectively.

Table 2. Detailed parameters of uniaxial compression test (A, B represent machined from Sample A, B).

Specimen No.	*d,* mm	*l,* mm	Gradient thickness, mm
1-6(A), 2-6(B)	12.5	25	0(without torsion)
1-1(A), 2-1(B)	5	10	2.5
1-2(A), 2-2(B)	8	16	4.0
1-3(A), 2-3(B)	11	22	5.5
1-4(A), 2-4(B)	12.5	25	6.25

Uniaxial compression tests were carried out on a computer controlled servo-hydraulic testing machine (INSTRON 8501). The compressive strain and stress are simultaneously recorded by the testing machine during the compression test.

Results and Discussion

Microstructure Observation

Metallographic structure of torsioned samples A and B are given in Fig.4. It can be found that the microstructure of both sample A and B consisted of equiaxed grains. The grain size was measured as the mean linear intercept and converted to true grain diameter, d, by $d = 1.68\bar{l}$.

The average grain diameters are 42.3μm and 41.5 μm for the centre regions of sample A and B, respectively. It is worth to note that the average grain diameters for the outermost region of sample A and B are 39.8μm and 40.6 μm, which is close to the grain size of centre regions. These results indicate that there is no obvious grain size gradient along the radial direction of the torsioned samples A and B.

The result of orientation image microscopy (OIM) with a scanning step size of 0.1μm for the outermost region of sample B, which has be subjected to 720° twisted deformation, is shown in Fig.

5(a). The microstructure very clearly shows the presence of coarse equiaxed grains. However, the crystal orientation distribution in each coarse grain is quite heterogeneous: many lamellar sub-grains can be found in the individual coarse grains.

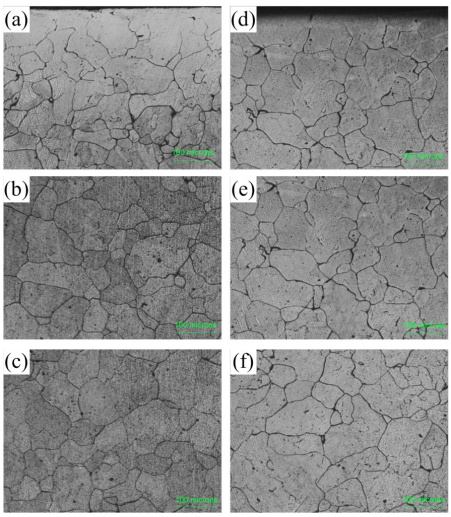

Note: (a), (d) are the outermost region of sample A and B, respectively; (b), (e) are the subsurface region of sample A and B, respectively. (c), (f) are the centre region of sample A and B, respectively.

Figure 4. Metallographic structure distribution along the radial direction of torsioned samples A and B.

The corresponding kernel average misorientation (KAM), which represents the local dislocation density distribution resulted by twisted deformation are presented in Fig. 5(b). Obviously, the local dislocation density distribution is non-uniform along the radial direction: the KAM values gradually decrease as the distance from top surface increases. This result corresponds well with the shear strain gradient distribution along the radial direction during twisted deformation.

The grain-subgrain boundary (GSB) map for the outermost region of sample B is shown in Fig. 5(b). In the GSB map, the red, green and blue lines represent the low angle boundaries (<5°) (LAB), medium angle boundaries (between 5° and 15°) (MAB) and high angle boundaries (>15°) (HAB), respectively. A relatively high density of subgrain boundaries (SBs) are detected in the coarse equiaxed grains.

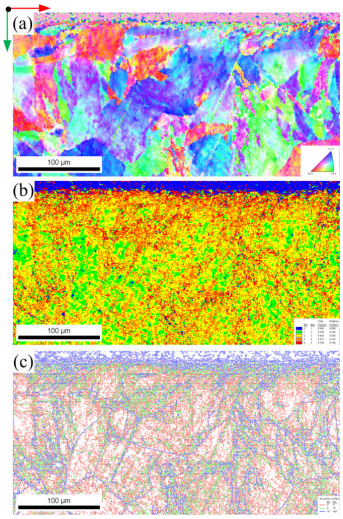

Note: (a) inverse pole figure (IPF) colored map, color code: Z direction; scanning step size: 0.1 lm. (b) Corresponding kernel average misorientation. (c) Corresponding grain-subgrain boundary (GSB) map.

Figure 5. Orientation image microscopy and grain boundaries map for the outermost region of sample B.

Furthermore, the distribution of total density of subgrain boundaries, including low angle boundaries (<5°) (LAB) and medium angle boundaries (between 5° and 15°) (MAB), which is related to local dislocation density are also presented an obvious gradient character, as shown in Fig.6. The LAB densities gradually decreased from ~1.1×10^5μm/cm^2 to 0.4×10^5 μm/cm^2, and the MAB densities decreased from ~1.6×10^5μm/cm^2 to 0.9×10^5 μm/cm^2, when the distance from top surface increase from 0 to 140μm. Correspondingly, the total density of subgrain boundaries is also gradually decreased from ~2.7×10^5μm/cm^2 to 1.4×10^5 μm/cm^2.

The microstructure analysis indicates that there is no obvious gradient in grain size of the twisted pure nickel sample. However, the remarkable dislocation density gradient along the radial direction has been produced after serious twisted deformation.

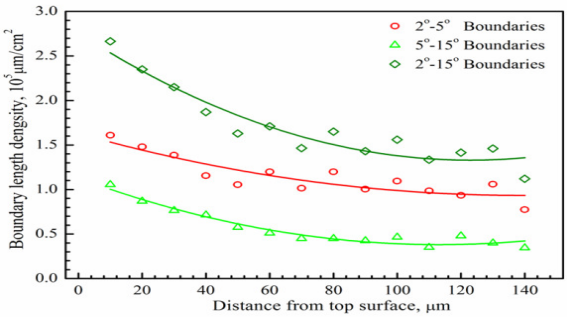

Figure 6. Gradient distribution of subgrain boundary density along the radial direction for the outermost region of sample B.

Micro Hardness Gradient

The variation of micro hardness of the sample A and B along the radial direction are shown in Fig.7 (a) and (b), respectively. The hardness present an obvious gradient distribution from top surface to centre region: it is gradually decreased along the radial direction.

In the centre region, where the shear strain is close to zero during the twisted deformation, the micro hardness value is around 1.3GPa. However, the micro hardness values are gradually increased and reach to 1.92GPa and 1.96GPa at the top surface region of sample A and B, respectively.

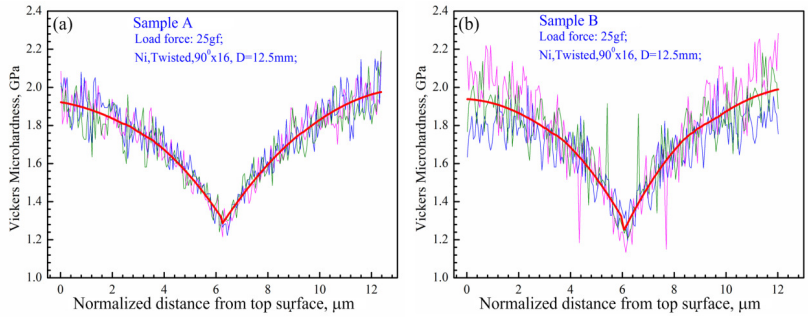

Figure 7. Gradient distribution of micro hardness along the radial direction (a) Sample A, (b) Sample B.

Obviously, the micro hardness gradient distribution is related to the shear strain gradient distribution along the radial direction during twisted deformation. These results correspond well with the kernel average misorientation and subgrain boundary density gradient distribution along the radial direction, which is related to local dislocation density.

Plastic Deformation Behavior

Uniaxial compression test are carried on the specimens with different gradient layer thickness machined from sample A and B and the stress-strain curves are shown in Fig.8 a and b, respectively.

The stress-strain behaviors shown in Fig. 8 a and b indicate that the yielding strength substantial increases as the gradient layer thickness increases.

For sample A, the yielding strength increases from 183MPa to 521MPa as the gradient layer thickness increases from zero (without twisted deformation) to 6.25mm. For sample B, which is subjected to a more serious twisted deformation, the highest yielding strength reaches to 618MaPa see curves 2-4 in Fig. 8 b). It is worth to note that, both in sample A and B, the gaps between adjacent two stress-strain curves are gradually decreased as the gradient layer thickness increases. This phenomenon indicates that the working hardening ability is gradually weakened with gradient layer thickness increase.

The work hardening rate-true strain curves for the specimens with different gradient layer thickness machined from sample A and B are presented by Fig. 8 c and d, respectively. It is clear to see that the samples without gradient layer possess excellent working hardening ability. The work hardening rate-true strain curves slowly decreased as the strain increases. However, for the samples with different gradient layer, the work hardening rate-true strain curves are sharply decreased, as seen the curves 1-1, 1-2, 1-3, 1-4 ,2-1, 2-2, 2-3 and 4-4 in Fig. 8 c and d, respectively.

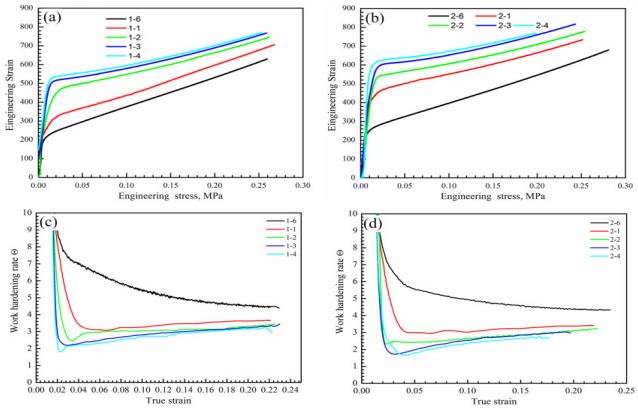

Note: (a), (b), Stress-strain curves of samples with different gradient layer thickness machined from sample A and B, respectively. (c), (d), work hardening rate-true strain curves of samples with different gradient layer thickness machined from sample A and B, respectively.

Figure 8. Stress-strain curves and work hardening rate-true strain curves for the twisted pure nickel sample A and B.

However, we also must note that, with gradient layer thickness increasing, the working hardening behaviors are much different. For samples 1-6 and 2-6 (without gradient layer), the work hardening rate-true strain curves is continuously decreased. For samples 1-1 and 2-1(with 2.5mm thickness gradient layer), the work hardening rate-true strain curves are sharply decreased firstly and then remain essentially flat. With gradient layer thickness further increasing, the “up-turn” phenomenon is presented: the work hardening rate-true strain curves are sharply decreased firstly and then slowly increase again, as seen curves 1-2, 1-3,1-4, 2-2, 2-3 and 2-4 in Fig.8 c and d, respectively. This work hardening ability re-obtained phenomenon is also found in nano-microstructure gradient material, such as grain size gradient [14], graded nanotwinned structure [8] and is believed induced by a special “gradient effect”. The current results firstly indicate that the materials which just contains pure dislocation density gradient also have this special “gradient effect”, which means that the pure dislocation density gradient can result in hardening ability re-obtained phenomenon.

Conclusions

(1) The grain size distribution along the radial direction of the torsioned cylindrical pure nickel samples is uniform: average grain diameters are 42.3μm and 41.5μm for the centre regions and 39.8μm and 40.6 μm for centre regions of sample A and B.

(2) The KAM values and subgrain boundaries density which is related to dislocation density are decreased along the radial direction.

(3) The micro hardness is gradually decreased from 1.92GPa and 1.96GPa to 1.3GPa for sample A and B, respectively.

(4) Yielding strength increases from 183MPa to 521MPa and 618MPa for sample A and B, respectively. The dislocation density gradient can also result in work-hardening rate "up-turn" phenomenon which is named "gradient effect".

Acknowledgement

The author (He Dong) gratefully acknowledges the financial support by National Natural Science Foundation of China under contract (No. 51401226), Outstanding Young Scholars Foundation (XN071010) and Startup FundProgram of North China University of Technology.

References

[1] M.A. Meyers, A. Mishra, D.J. Benson, Mechanical properties of nanocrystalline materials, Prog. Mater. Sci., 51 (2006) 427-556.

[2] C.C. Koch, Optimization of strength and ductility in nanocrystalline and ultrafine grained metals, Scripta Mater., 49 (2003) 657-662.

[3] Y. Xin, M. Wang, Z. Zeng, M. Nie, Q. Liu, Strengthening and toughening of magnesium alloy by {1 0 −1 2} extension twins, Scripta Mater., 66 (2012) 25-28.

[4] X.Y. Zhang, Y.T. Zhu, Q. Liu, Deformation twinning in polycrystalline Co during room temperature dynamic plastic deformation, Scripta Mater., 63 (2010) 387-390.

[5] J.Y. Zhang, G. Liu, X. Zhang, G.J. Zhang, J. Sun, E. Ma, A maximum in ductility and fracture toughness in nanostructured Cu/Cr multilayer films, Scripta Mater., 62 (2010) 333-336.

[6] P. Zhang, X.H. An, Z.J. Zhang, S.D. Wu, S.X. Li, Z.F. Zhang, R.B. Figueiredo, N. Gao, T.G. Langdon, Optimizing strength and ductility of Cu–Zn alloys through severe plastic deformation, Scripta Mater., 67 (2012) 871-874.

[7] T.H. Fang, W.L. Li, N.R. Tao, K. Lu, Revealing Extraordinary Intrinsic Tensile Plasticity in Gradient Nano-Grained Copper, Science, 331 (2011) 1587-1590.

[8] Y. Wei, Y. Li, L. Zhu, Y. Liu, X. Lei, G. Wang, Y. Wu, Z. Mi, J. Liu, H. Wang, H. Gao, Evading the strength–ductility trade-off dilemma in steel through gradient hierarchical nanotwins, Nat. Commun., 5 (2014) 3580.

[9] H.W. Zhang, Z.K. Hei, G. Liu, J. Lu, K. Lu, Formation of nanostructured surface layer on AISI 304 stainless steel by means of surface mechanical attrition treatment, Acta Mater., 51 (2003) 1871-1881.

[10] X.C. Liu, H.W. Zhang, K. Lu, Strain-Induced Ultrahard and Ultrastable Nanolaminated Structure in Nickel, Science, 342 (2013) 337-340.

[11] Y.F. Shen, L. Lu, Q.H. Lu, Z.H. Jin, K. Lu, Tensile properties of copper with nano-scale twins, Scripta Mater., 52 (2005) 989-994.

[12] X. Wu, M. Yang, F. Yuan, G. Wu, Y. Wei, X. Huang, Y. Zhu, Heterogeneous lamella structure unites ultrafine-grain strength with coarse-grain ductility, P. Natl. Acad. Sci., 112 (2015) 14501-14505.

[13] A.W. Thompson, W.A. Backofen, Production and mechanical behavior of very fine-grained copper, Metall. Trans., 2 (1971) 2004-2005.

[14] K. Lu, Making strong nanomaterials ductile with gradients, Science, 345 (2014) 1455-1456.